Snowmass Energy Frontier Simulations

Conveners: Sergei Chekanov, Sanjay Padhi

Jacob Anderson[2], Aram Avetisyan[1], Raymond Brock[3], Sergei Chekanov[4], Timothy Cohen[5], Nitish Dhingra[6], James Dolen[14], James Hirschauer[2], Kiel Howe[7], Ashutosh Kotwal[8], Tom LeCompte[4], Sudhir Malik[9], Patricia Mcbride[2], Kalanand Mishra[2], Meenakshi Narain[10], Jim Olsen[11], Sanjay Padhi[12], Michael E. Peskin[5], John Stupak III[13], and Jay G. Wacker[5]

[1] Boston University, Boston, MA, USA
[2] Fermi National Accelerator Laboratory, Batavia, USA
[3] Michigan State University East Lansing, MI, USA
[4] Argonne National Laboratory, Argonne, USA
[5] SLAC National Accelerator Laboratory, Menlo Park, USA
[6] Panjab University, Chandigarh, India
[7] Stanford Institute for Theoretical Physics, Stanford University, Stanford, USA
[8] Duke University, Durham, USA
[9] University of Nebraska-Lincoln, Lincoln, USA
[10] Brown University, Providence, USA
[11] Princeton University, Princeton, USA
[12] University of California, San Diego, USA
[13] Purdue University Calumet, Hammond, USA
[14] SUNY Buffalo, USA

This document describes the simulation framework used in the Snowmass Energy Frontier studies for future Hadron Colliders. An overview of event generation with MADGRAPH5 along with parton shower and hadronization with PYTHIA6 is followed by a detailed description of pile-up and detector simulation with DELPHES3. Details of event generation are included in a companion paper cited within this paper. The input parametrization is chosen to reflect the best object performance expected from the future ATLAS and CMS experiments; this is referred to as the "Combined Snowmass Detector". We perform simulations of pp interactions at center-of-mass energies $\sqrt{s} = 14$, 33, and 100 TeV with 0, 50, and 140 additional pp pile-up interactions. The object performance with multi-TeV pp collisions are studied for the first time using large pile-up interactions.

1.1 Introduction

The Large Hadron Collider (LHC) at CERN, which collided protons at $\sqrt{s} = 8$ TeV center-of-mass energy in 2012, is the most powerful particle accelerator ever built and the forefront of the energy frontier. The ATLAS [1] and CMS [2] multipurpose detectors record the pp collisions of the LHC, reconstructing decay products with excellent efficiency and resolution. For precise analysis of collision data, the ATLAS and CMS collaborations fully simulate interactions of particles with their detectors using GEANT4 [3]. In addition, the collaborations use sophisticated algorithms for reconstruction of events, particles, and physical quantities in simulated and collision data.

Long-term planning studies in high energy physics, which seek to compare various scenarios of center-of-mass energy, numbers of pp interactions per bunch crossing (pile-up), and integrated luminosity, require a fast and realistic estimation of the expected detector performance as a function of these variables. In this context, we use simulation parameters that are expected to reflect the best expected performance from the ATLAS and

Operated by Fermi Research Alliance, LLC under Contract No. De-AC02-07CH11359 with the United States Department of Energy.

CMS detectors, this is referred to as the "Combined Snowmass LHC detector". The Combined Snowmass LHC detector and the simulations based on it are meant to provide a single transparent fast-simulation framework for studies of the capabilities of hadron collider experiments at 14, 33, and 100 TeV, including effects due to in-time pile-up at high luminosity. This framework uses the DELPHES [4] fast-simulation model with inputs from publicly available detector and performance parameters [5, 6, 7, 8] that were expected, in the spring of 2013, to reflect the best performance of the future ATLAS and CMS sub-detector components. The framework does not take into account the subsequent evolution of the ATLAS and CMS detector designs, and it is not at the level of a full detailed Geant-based simulation. Results derived from this framework are not official ATLAS or CMS simulation results and should not be considered on the same footing.

The main goal of the present long-term planning exercise, the Snowmass Community Summer Study, is to fully develop the long-term physics aspirations of the community. The Snowmass narrative will communicate the opportunities for discovery in high energy physics to the broader scientific community and to the United States government. The studies associated with the energy frontier address the physics potential of *pp* interactions at $\sqrt{s}$ =14, 33 and 100 TeV with 0, 50 and 140 pile-up interactions, and integrated luminosities of 300 and 3000 fb^{-1}. A bunch spacing of 25 ns is assumed for these studies.

Section 1.2 discusses future hadron collider scenarios and the expected luminosity evolution. In Sec. 1.3, we describe simulation tools including the background processes in Sec. 1.3.1 and DELPHES in Sec. 1.3.3. In Sec. 1.4, we describe the performance of the simulation, followed by summary and conclusion in Sec. 1.5.

1.2 Scenarios: Future hadron colliders and detectors

The energies and pile-up scenarios chosen for simulation are intended to represent real proposed hadron colliders. The upcoming LHC run, which includes the Phase I upgrades of the CMS and ATLAS detectors, is expected to provide 300 fb^{-1} of 14 TeV *pp* collisions with a mean $< \mu >$=50 pile-up interactions. The HL-LHC is planned to commence following a long shut down in 2022 and will provide 3000-fb^{-1} at 14 TeV over the following decade. Other proposed hadron colliders include the HE-LHC, which would use the same tunnel as the LHC with stronger dipole magnets to achieve 33 TeV *pp* collisions, and the VHE-LHC, which would require a new larger ring to produce 100 TeV *pp* collisions. Table 1-1 summarizes various hadron collider scenarios that are used in this study.

Parameter	LHC	HL-LHC	HE-LHC	VLHC
Energy [TeV]	14	14	33	100
Mean additional interactions per crossing ($< \mu >$)	50	140	140	140
Integrated Luminosity [fb^{-1}]	300	3000	3000	3000

Table 1-1. *Benchmark hadron collider scenarios under study with the simulated samples described in this document.*

We use the same basic detector parametrization for all of the collider scenarios. The Combined Snowmass Detector parametrization incorporates the performance of the best features of the existing LHC detectors and, the expected performance of the upgraded LHC detectors [5, 6, 7, 8]. A schematic overview of detector sub-components of the ATLAS and CMS detectors is shown in Fig. 1-1. As described in Sec. 1.3.3, the tracking and identification efficiencies are parametrized and input to DELPHES, while the isolation efficiency is not an input and is determined by the simulation.

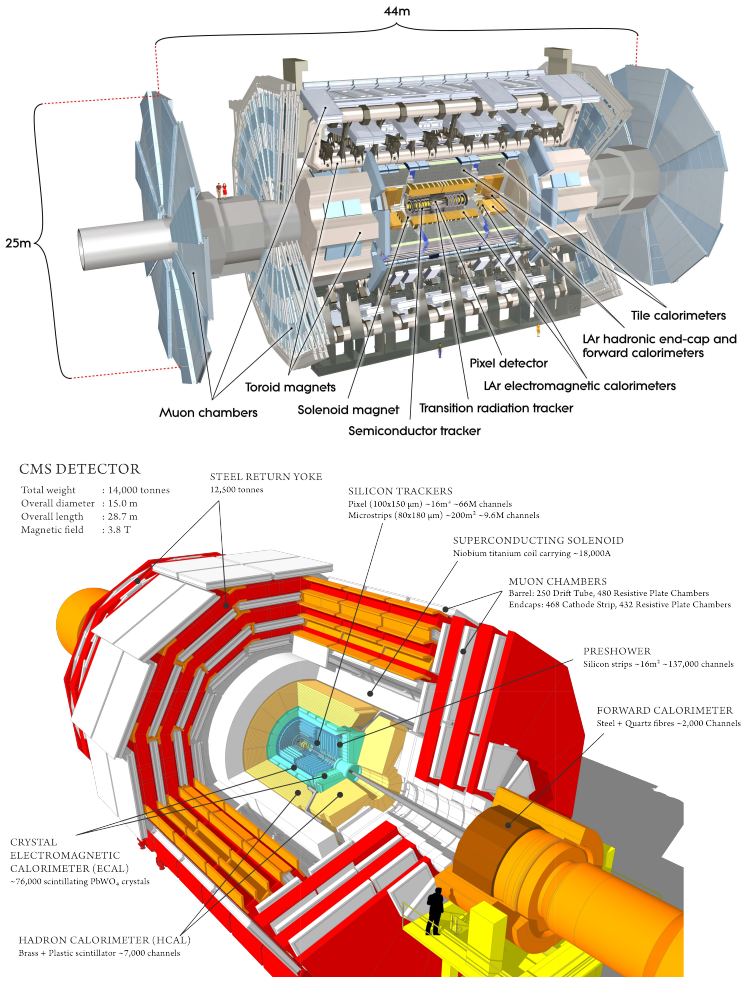

Figure 1-1. *Schematic overview of ATLAS and CMS detectors*

1.3 Simulation tools

We simulate a set of standard model (SM) processes that we expect will encompass the backgrounds for most new phenomena searches at the future colliders described in Table 1-1. The simulation procedure involves parton-level generation of events at leading order in bins of the scalar sum of the recoil jet p_{T} (H_{T}^{*}), particle decay, parton showering and hadronization, jet-parton matching, corrections for next-to-leading order (NLO) contributions, and detector simulation. In this section, we give an overview of the procedure and describe the detector simulation in detail; the details of all other stages can be found in Ref. [9, 10].

We use Madgraph5 [11] for event generation. To enhance numbers of events in boson decay modes, we use Bridge [12] to decay the generated bosons with equal probability to a set of allowed final states. For example, Z bosons decay with equal probability to pairs of quarks, neutrinos, electrons, muons, or tau leptons. Stable particles are passed to Pythia6 [13] for parton showering and hadronization. The Madgraph5 generated partons are appropriately matched to jets from Pythia6 at a given energy scale that depends on the process

to avoid overlap between phase-space descriptions. Each event has an associated weight that corrects for NLO contribution to the total cross section and the effects of branching ratio leveling. Because the NLO correction depends on the sub-process (e.g. W+jets or Z+jets) and the branching ratio on the decay mode (e.g. $Z \to \mu^+\mu^-$ or $Z \to q\bar{q}$), the weights are inserted at the event level and can be retrieved with the `Weight` method of the `Event` object in the output sample.

After generation, decay, parton showering, and hadronization, the stable particles are passed to Delphes for pile-up mixing, detector simulation, and object reconstruction. The Delphes steps are described in Sec. 1.3.3 after a brief description of the background processes and binning.

1.3.1 Background processes

The background processes all involve combinations of bosons (B = γ, W$^\pm$, Z), Higgs bosons (H), charged and neutral leptons (L), top quarks (t), and light quark jets (j). We summarize the processes in Table 1.3.2. For all samples (except B-4p) we generate four particles at parton level: the N particles specified in the dataset name with the remaining $4 - N$ particles generated as hadronic jets. The B-4p, Bj-4p, and Bjj-vbf-4p samples all include on-shell boson+jets processes and, being exclusive samples, are all required for full boson+jets simulation. The B-4p sample includes events with a boson plus zero generated jets; the Bj-4p sample includes events with a boson plus one to three generated jets; and the Bjj-vbf-4p sample includes events with a boson produced in association with at least two jets resulting from an off-shell electroweak process: either the usual t-channel vector boson fusion (VBF) diagrams or an off-shell s-channel vector boson decaying to jets. In practice, the Bjj-vbf-4p cross section is very small and can be neglected for analyses not concerned with the VBF topology. The LL samples include processes with off-shell W/Z and jets. Particles are considered on-shell if they are within 15 natural widths of the resonance mass.

1.3.2 Binning in H_{T}^*

These samples are intended for studies with integrated luminosity up to 3 ab^{-1}. To efficiently populate the full particle spectra for quantities such as p_{T}, invariant mass, and missing transverse energy ($E_{\mathrm{T}}^{\mathrm{miss}}$), we generate events in bins of H_{T}^*. Each process in Table 1.3.2 is generated in 5-7 bins of H_{T}^* depending on the process, and analysts must use all bins to correctly simulate the complete process. The binning and numbers of events generated are chosen so that the statistical uncertainty at all points in the H_{T}^* spectrum appropriate for studies at 3 ab^{-1} is much less than 30%. By binning in H_{T}^*, the numbers of events required are decreased from $\sim 10^{10}$ per process to 10^{6-7} per process. This binning process, including choice of bin boundaries, is described in detail in Ref. [9].

1.3.3 Delphes detector simulation

Delphes is a C++ framework for parametrized simulation of a general collider experiment. Starting from the output of an event generator, the framework propagates particles through the detector with a solenoidal magnetic field; applies tracking efficiency, reconstruction efficiency, and momentum resolution; and clusters hadronic jets with identification of those resulting from b quarks, τ leptons and decay products from t quarks, H, W and Z bosons.

Dataset name	Physics process	Number of recoil jets
B-4p	γ or on-shell W, Z	0
Bj-4p	γ or on-shell W, Z	1-3
Bjj-vbf-4p	γ or off-shell W, Z, H in VBF topology	2-3
BB-4p	Diboson (γ, W, Z) processes	0-2
BBB-4p	Tri-boson (γ, W, Z) processes including BH	0-1
LL-4p	Non-resonant dileptons (including neutrinos) with $m_{ll} > 20$ GeV	0-2
LLB-4p	Non-resonant dileptons with an on-shell boson, $m_{ll} > 20$ GeV	0-1
H-4p	Higgs	0-3
tj-4p	Single top (s- and t-channel)	0-2
tB-4p	Single top associated with a boson	0-2
tt-4p	$t\bar{t}$ pair production	0-2
ttB-4p	$t\bar{t}$ associated with γ, W, Z, H	0-1

Table 1-2. *Table of background processes. All processes include the particles in the dataset name plus additional recoil jets up to four generated particles. On-shell vector bosons, off-shell dileptons, Higgs bosons, top quarks, and jets are denoted B, LL, H, t, and j, respectively. In the Bjj-vbf-4p case, B includes Higgs. In the BBB-4p case, BBB includes BH. Samples are generated in bins of H_{T}^{*} for $\sqrt{s}$ = 14, 33, and 100 TeV.*

The detector simulation is composed of five primary components listed below. The ultimate efficiency and resolution for each object comes from the combination of these components:

- input tracking efficiency (for charge hadrons, electrons, and muons),
- input momentum resolution (for charge hadrons, electrons, and muons),
- input calorimeter resolution (for electromagnetic and hadron calorimeters),
- input reconstruction efficiency (for photons, electrons, and muons),
- and isolation (for photons, electrons, and muons), which is not input by the user but determined from the simulation.

The specific modules of the framework, their user inputs, and the values used for the Combined Snowmass Detector (denoted with square brackets []) are described below.

1.3.3.1 Delphes modules

- `PileUpMerger`
  Input: Name of file of minimum bias events to be mixed as pile-up, mean number of pile-up interactions per crossing [0, 50, or 140], Gaussian standard deviation of the bunch length (in the z direction) in meters [0.05m].
  Function: Stable particles from minimum bias pile-up events are mixed with the final state particles from the generated event with the given z distribution.

- `ParticlePropagator`:
  Input: Radius [1.2m], length [6m], and magnitude [3.8T] of solenoidal magnetic field.
  Function: Stable particles (including unsubtracted pile-up) are classified as charged hadrons, electrons, or muons and propagated through the solenoidal magnetic field.

- `ChargedHadronTrackingEfficiency`:
  Input: Efficiency for tracking of charged hadrons as a function of pseudorapidity η and p_T [Table 1-3].
  Function: Tracking efficiency is applied to propagated charged hadrons.

- `ElectronTrackingEfficiency`:
  Input: Efficiency for tracking of electrons as a function of η and p_{T} [Table 1-3].
  Function: Tracking efficiency is applied to propagated electrons.

- `MuonTrackingEfficiency`:
  Input: Efficiency for tracking of muons as a function of η and p_{T} [Table 1-3].
  Function: Tracking efficiency is applied to propagated muons.

- `ChargedHadronMomentumSmearing`:
  Input: Momentum resolution for charged hadron as a function of η and p_{T} [Table 1-4].
  Function: Momentum of propagated charged hadrons is smeared according to resolution.

- `ElectronMomentumSmearing`:
  Input: Momentum resolution for electrons as a function of η and E [$\sigma_{p_{\mathrm{T}}} = 1.5\% \cdot E$ for electron energy less than 25 GeV and $\sigma_{p_{\mathrm{T}}} = \sqrt{(0.5\%)^2 \cdot E^2 + (2.7\%)^2 \cdot E + (15\%)^2}$ for electron energy greater than 25 GeV].
  Function: Momentum of propagated electrons is smeared according to resolution.

- `MuonMomentumSmearing`:
  Input: Momentum resolution for muons as a function of η and p_T [Table 1-4].
  Function: Momentum of propagated muons is smeared according to resolution.

- `Calorimeter`:
  Input: Energy resolution as function of η and energy for electromagnetic and hadronic energy measurements. Segmentation in η and ϕ of calorimeter towers.
  Function: Charged hadrons, muons, electrons, and other stable particles are combined into `EFlow` tracks and towers. Tower energy is smeared by the input energy resolutions.

- `TrackPileUpSubtractor`:
  Input: Resolution on z-position of primary vertex [0.1cm].
  Function: Charged particles with z-position of point of closest approach in the x-y plane greater than the input resolution on z-position are rejected as pile-up.

- `PhotonEfficiency`:
  Input: Photon reconstruction efficiency as a function of η and p_T [Table 1-5].
  Function: Reconstruction efficiency is applied to photons.

- `ElectronEfficiency`:
  Input: Electron reconstruction efficiency as a function of η and p_T [Table 1-5].
  Function: Reconstruction efficiency is applied to electrons.

- `MuonEfficiency`:
  Input: Muon reconstruction efficiency as a function of η and p_T [Table 1-5].
  Function: Reconstruction efficiency is applied to muons.

- `PhotonIsolation`:
  Input: Cone size [0.3] and threshold on energy ratio for photon relative isolation [0.1].
  Function: Isolation requirement is applied to photons.

- `ElectronIsolation`:
  Input: Cone size [0.3] and threshold on energy ratio for electron relative isolation [0.1].
  Function: Isolation requirement is applied to electrons.

- `MuonIsolation`:
  Input: Cone size [0.3] and threshold on energy ratio for muon relative isolation [0.1].
  Function: Isolation requirement is applied to muons.

- `FastJetFinder`:
  Input: Jet algorithm [anti-k_T [15]] and relevant parameters [distance parameter = 0.5] (AK5).
  Function: `EFlow` tower and track collections from the `Calorimeter` stage and muons are clustered into jets. Jet area is computed and stored.

- `JetPileUpSubtractor`:
  Function: The jet four-vector is corrected for contributions from neutral pile-up using FastJet ρ subtraction [14].

- `BTagging`:
  Input: Efficiency to identify a true b-jet as having come from a b quark (b-tag) as function of η and p_T. Probability to misidentify a light flavor jet as having come from a b quark (mistag rate). [Figs. 1-14-1-17].
  Function: Clustered jets are identified as having come from a b quark. Multiple working points can be evaluated for each jet.

- `TauTagging`:
  Input: Efficiency to identify a true τ-jet as having come from a τ lepton (τ-tag) as function of η and p_T [65% flat in η and p_T]. Probability to misidentify a jet as having come from a τ lepton (mistag rate) [0.4% flat in η and p_T].
  Function: Clustered jets are identified as having come from a τ.

- `UniqueObjectFinder` : **Function**: Overlapping particles are removed from collections as appropriate. For instance, photons are removed from electron collections.

- `TreeWriter` : **Function**: Desired output is written to an output file.

Object	p_{T} range	$\lvert\eta\rvert \leq 1.5$	$1.5 < \lvert\eta\rvert \leq 2.5$
Charged Hadron	> 1 GeV	97.0%	90.0%
Electron	$1 - 100$ GeV	97.0%	90.0%
Electron	> 100 GeV	99.0%	95.0%
Muon	> 1 GeV	99.9%	98.0%

Table 1-3. *Tracking efficiency for charged hadrons, electrons, and muons.*

p_{T} range	$\lvert\eta\rvert \leq 1.5$	$1.5 < \lvert\eta\rvert \leq 2.5$
$1 - 10$ GeV	1.3%	1.5%
$10 - 200$ GeV	2.0%	4.0%
> 200 GeV	5.0%	5.0%

Table 1-4. *p_{T} resolution for charged hadrons and muons.*

Object	$\lvert\eta\rvert \leq 1.5$	$1.5 < \lvert\eta\rvert \leq 2.5$
Photon	96.4%	96.2%
Electron	98.0%	90.0%
Muon	99.0%	97.0%

Table 1-5. *Reconstruction efficiency for photons, electrons, and muons. The upper limit of the η range is 2.4 for muons.*

1.3.3.2 Pile-up mixing and subtraction

Delphes simulates the pile-up expected with higher luminosity by mixing additional minimum bias interactions with the original generated event. We address scenarios of $< \mu >$=0, 50 and 140 pile-up interactions for each $\sqrt{s}$ = 14, 33, and 100 TeV.

Minimum bias events that are expected with a "loose" trigger that accepts a large fraction of the overall inelastic pp interactions are produced using CMS $Z2^*$ Pythia tune. Pile-up events are randomly selected from the minimum bias sample and are mixed with the event from the primary interaction according to a Poisson distribution with a mean of 0, 50, or 140 additional interactions. These events are randomly distributed along the beam axis according to a Gaussian distribution with a width of 0.05 m.

If the z-position of a pile-up vertex is less than the 0.1 cm vertex resolution. the pile-up interaction cannot be separated from the additional vertices. For such vertices, all particles from both the pile-up and primary interactions are included in the object reconstruction. For pile-up interactions with z-vertex position greater than the resolution, subtraction of charged pile-up particles within the tracker volume is applied with an efficiency of unity. We use the FastJet area method [14] to correct measurements of jet four-vectors and isolation energy for contribution from neutral pile-up particles and charged pile-up particles outside the tracker acceptance.

In Fig. 1-2, we show the detector response to jets in simulated events using QCD processes. The response is shown as a function of η and p_{T} for 0, 50, 100, and 140 pile-up interactions before and after pile-up subtraction. The subtraction removes the pile-up dependence on average with some residual η dependence. Residual off-set corrections are applied to events with large pile-ups in bins of η and p_T to recover the jet energy response as in the case of 0 pile-up scenario.

1.3.3.3 Jet substructure

In the past several years, there has been significant development of techniques for discriminating between new phenomena and the large SM background with the substructure of jets. When particles decaying to jets (such as top quarks, W, Z, and Higgs bosons) have sufficient Lorentz boost in the lab frame, their jet

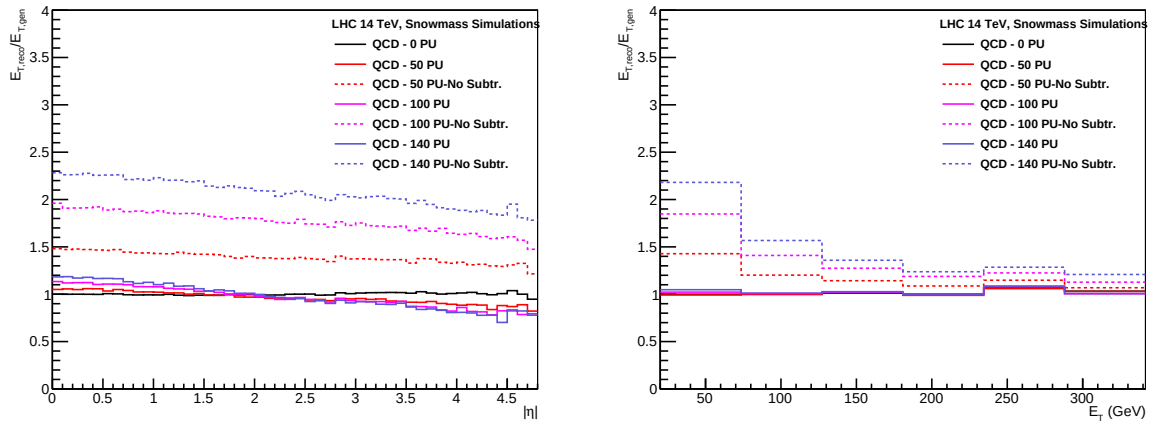

Figure 1-2. *Jet response in QCD events as a function of $|\eta|$ (left) and p_T (right) for 0, 50, 100 and 140 pile-ups, before and after pile-up subtraction.*

daughters overlap in the detector and are more likely to be reconstructed as a single jet than as two or more jets. Recognizing that this overlap is possible it is important to use discriminants for classifying boosted new phenomena and SM backgrounds.

We have added functionality to the FastJetFinder module that *(i)* computes and saves variables useful for jet substructure studies and *(ii)* flags jets as having come from a top quark or H, Z, W bosons. We compute these variables and flags for jets clustered with the the Cambridge-Aachen algorithm [16] with a distance parameter of 0.8 (CA8); this jet collection is in addition to the basic anti-k_{T} jet collection with distance parameter of 0.5. The saved variables are trimmed jet mass, τ_1, τ_2, τ_3, N_{subjets}, and mass drop. The flags are based on trimmed jet mass and N_{subjets} for top identification, and trimmed jet mass and mass drop for W and Higgs identification. The trimmed jet parameter values are p_T fraction of 0.5 and CA distance parameter of 0.2.

The variables used in top- and W-tagging were chosen because of their pile-up stability in order to minimize pile-up dependence of the requirements on these variables and the tagging efficiency itself. The N-subjettiness variables (τ_3, τ_2, τ_1) were not used in the taggers because they exhibit pile-up dependence, but they are included in the output `Jet` object for analysis-level jet tagging.

1.4 Simulation performance

In this section we show the output of the full simulation procedure with focus on the effects of pile-up. We show basic spectra for missing energy, H_{T} (scalar sum p_T of the jets), electrons, and muons; reconstruction efficiency for electrons, muons, and photons; jet substructure variables; and efficiencies and fake rates for tagging of b quarks, τ leptons, t quarks, and W bosons.

The performance is evaluated in $t\bar{t}$+jets and boson+jets events with $\sqrt{s} = 13$ TeV and $\sqrt{s} = 14$ TeV and three pile-up scenarios. We require at least four jets with $p_{\mathrm{T}} > 30$ GeV and $|\eta| < 2.5$ and one electron (muon) with $p_{\mathrm{T}} > 30(20)$ GeV and $|\eta| < 2.5$; when evaluating photon efficiency we replace the lepton requirement with a requirement for a photon with $p_{\mathrm{T}} > 20$ GeV and $|\eta| < 2.5$.

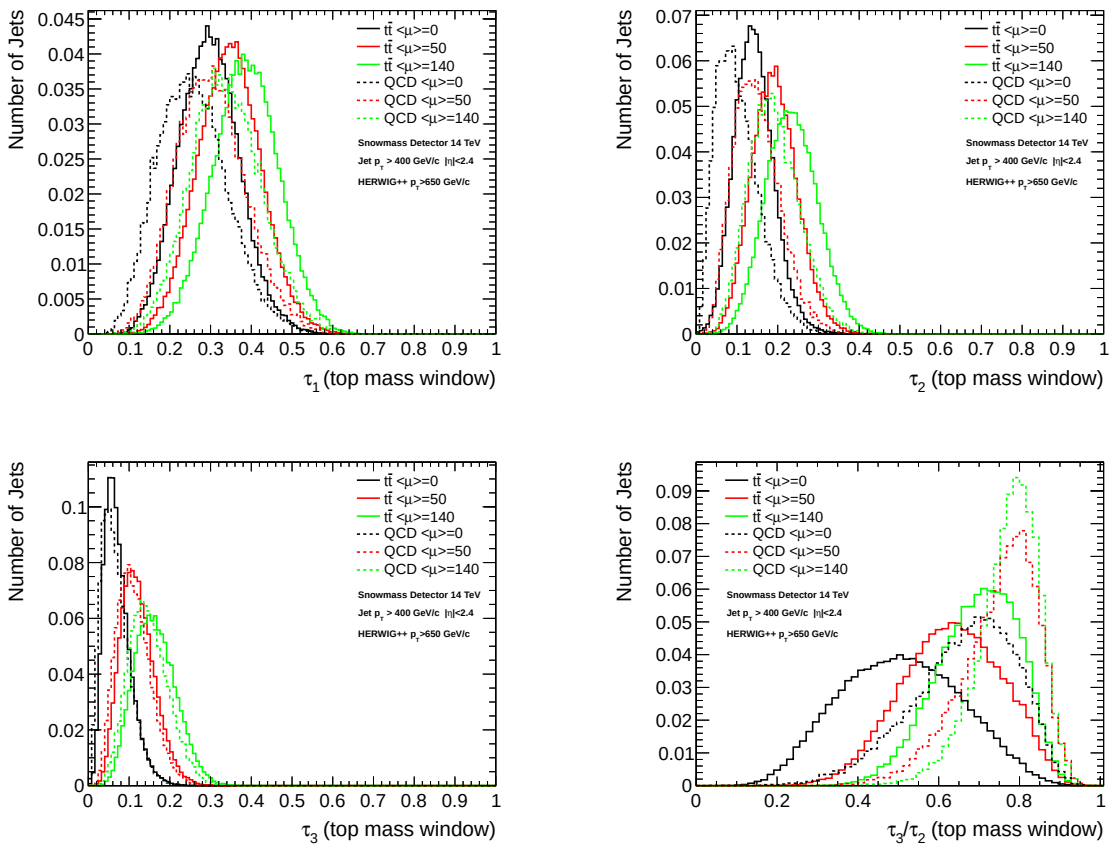

Figure 1-3. *N-subjettiness variables τ_1 (top left), τ_2 (top right), τ_3 (bottom left), and τ_3/τ_2 (bottom right) in $t\bar{t}$+jets and QCD events with 0, 50, and 140 pile-up.*

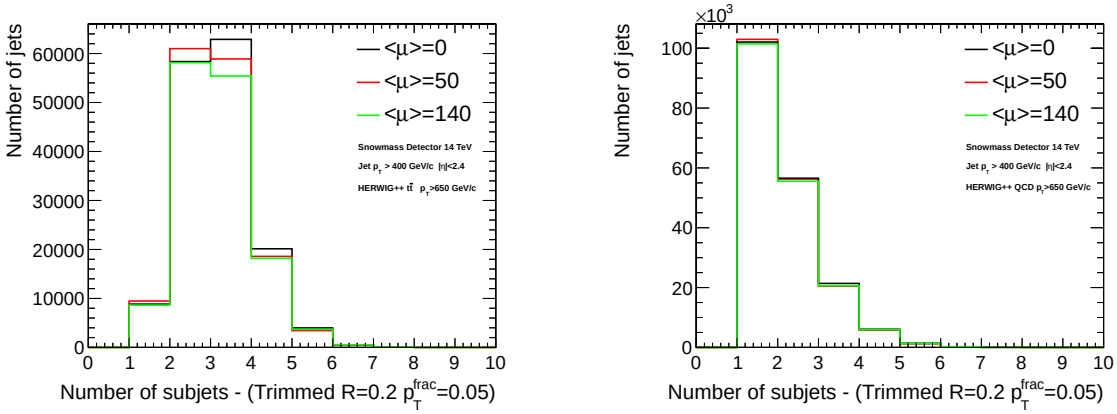

Figure 1-4. *N-subjets in $t\bar{t}$+jets (left) and QCD events (right) with 0, 50, and 140 pile-up.*

1.4.1 Jet and $E_{\mathrm{T}}^{\mathrm{miss}}$ performance

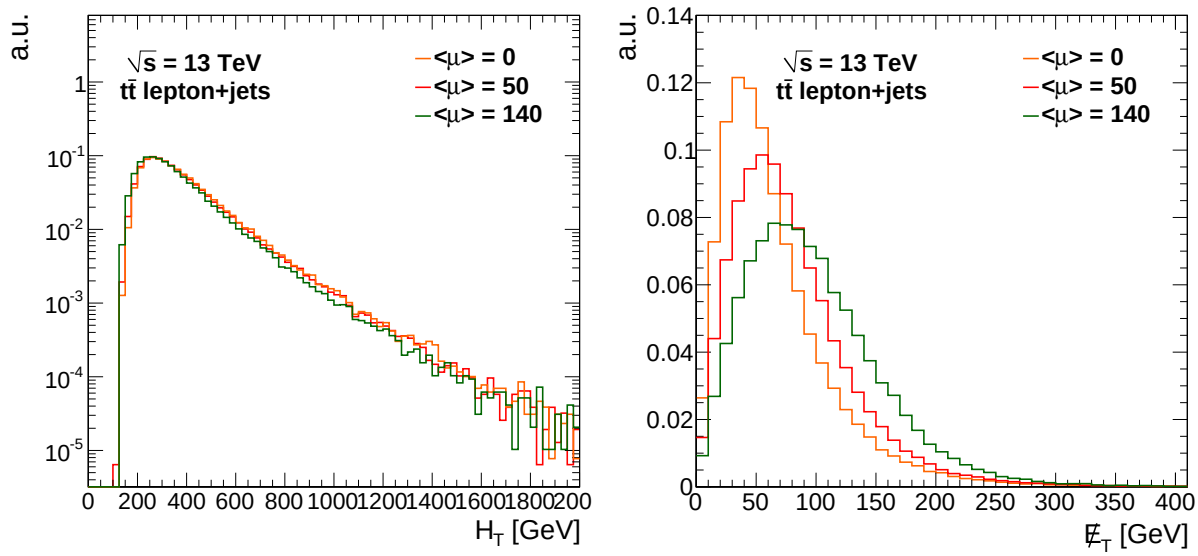

Figure 1-5. *Event H_{T} (left) and $E_{\mathrm{T}}^{\mathrm{miss}}$ (right).*

In Fig. 1-5, we show the scalar sum of the p_{T} of jets with p_{T}>30 GeV and $|\eta|$ <2.5 (H_{T}) and the event $E_{\mathrm{T}}^{\mathrm{miss}}$. The H_{T} distribution exhibits less pile-up dependence than the $E_{\mathrm{T}}^{\mathrm{miss}}$ distribution mainly because H_{T} is computed from jets that are pile-up subtracted and pass the p_{T} threshold requirement. However, the $E_{\mathrm{T}}^{\mathrm{miss}}$ is computed using all event objects (with minimal thresholds) in order to maintain an unbiased response to missing energy. Computing missing energy from jets passing a p_{T} threshold (often called missing H_{T}) minimizes pile-up dependence, but can have bias in $E_{\mathrm{T}}^{\mathrm{miss}}$ response at lower thresholds.

In Fig. 1-6, we show distributions for jet p_{T} and multiplicity. The effect of pile-up even after subtraction can be observed in the additional number of jets in the distribution. In this forward detector region, where there is no acceptance due to tracking, both neutral and charged pile-up interactions are subtracted using average ρ area method.

The jet energy resolution as a function of p_{T} and various pile-up scenarios is shown in Fig. 1-7. The impact of pile-up is evident from the increase in the "noise" term in the resolution function.

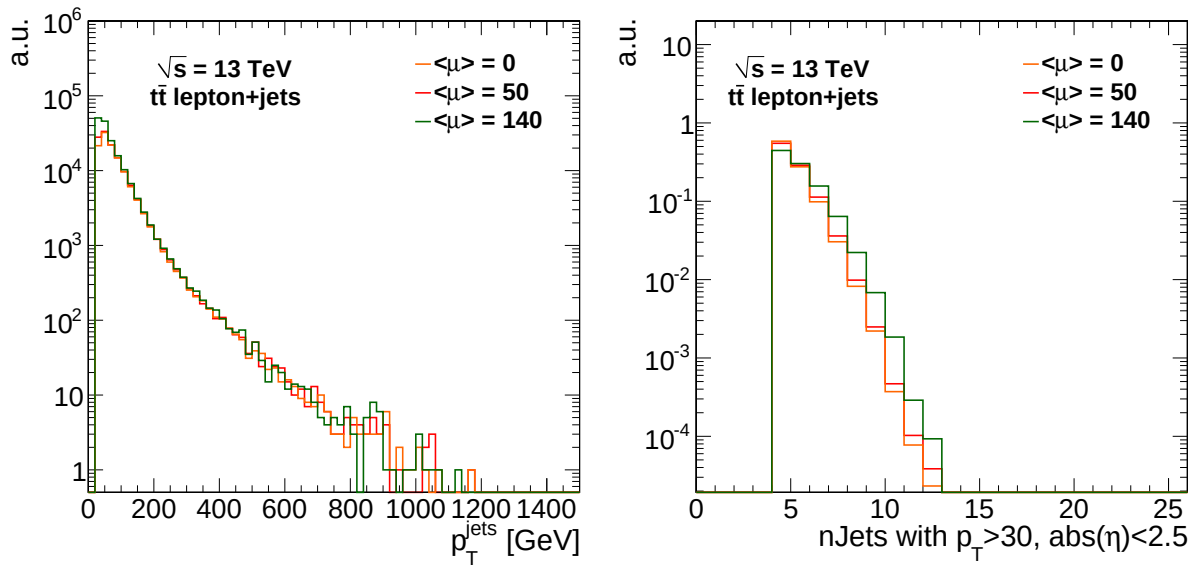

Figure 1-6. *Jet p_T (top left) and multiplicity (right) distributions.*

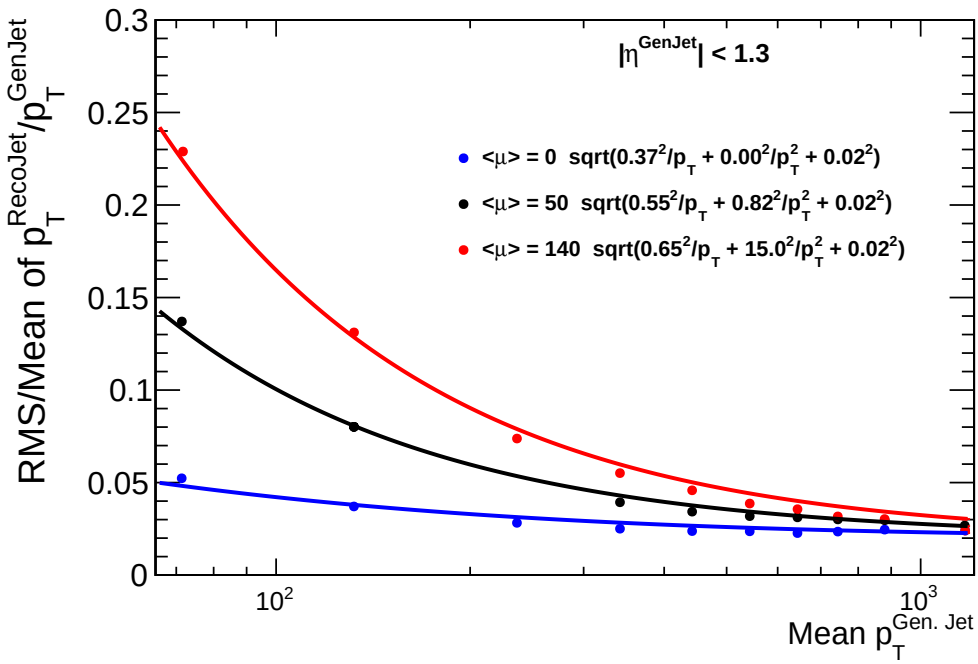

Figure 1-7. *Jet energy resolution as a function of jet p_T.*

1.4.2 Lepton and photon performance

The lepton p_T and η distributions are shown in Fig. 1-8. They exhibit milder pile-up dependence due to the subtraction used. Fig. 1-9 shows the resulting efficiencies for leptons that pass reconstruction and isolation requirements. These efficiencies result from the combined effects of tracking efficiency, reconstruction efficiency, resolution, and isolation. In Fig. 1-10, we show lepton efficiency with no isolation requirement. These are used as inputs with extrapolations using the LHC data [xx].

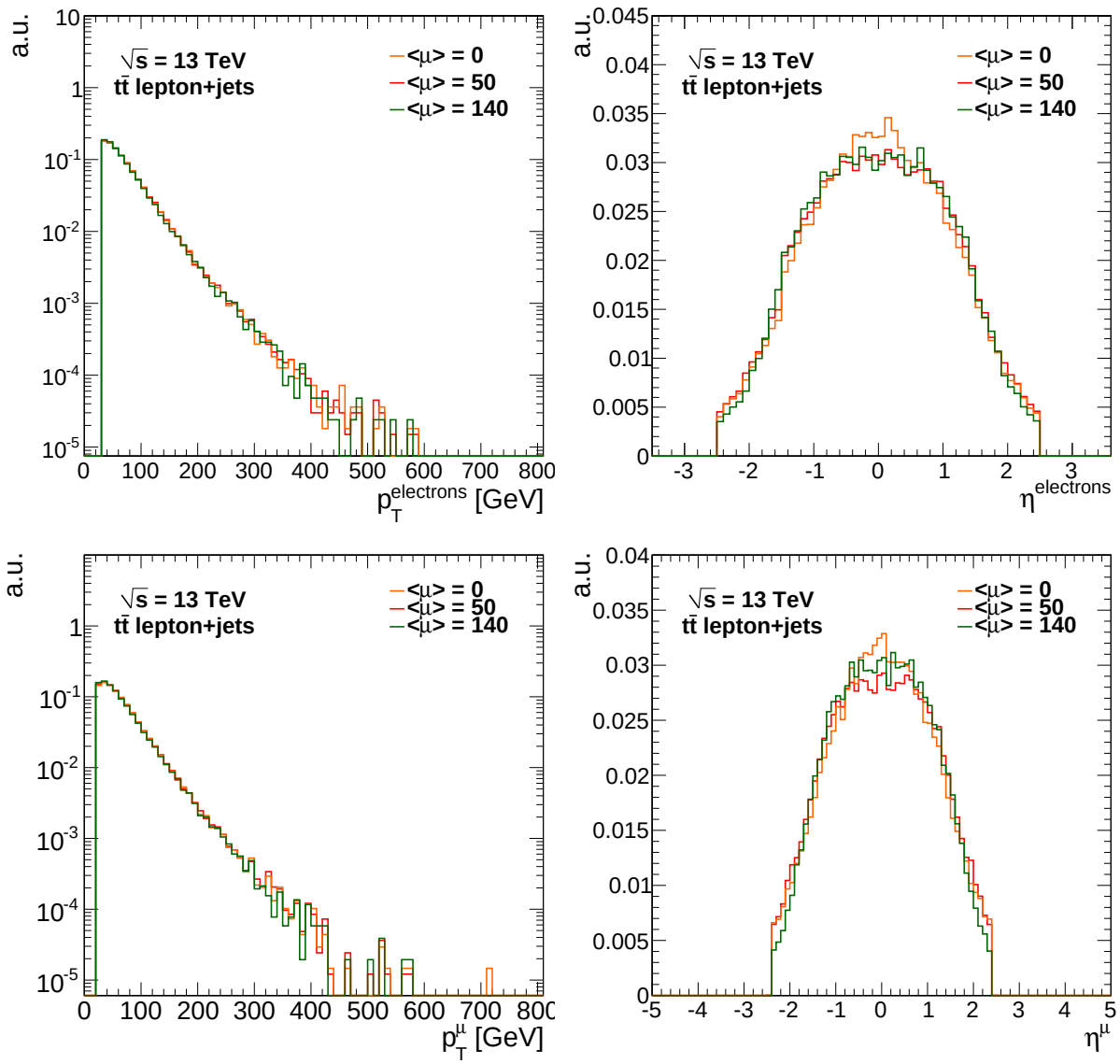

Figure 1-8. *Distributions for p_T (left) and η (right) for electrons (top) and muons (bottom).*

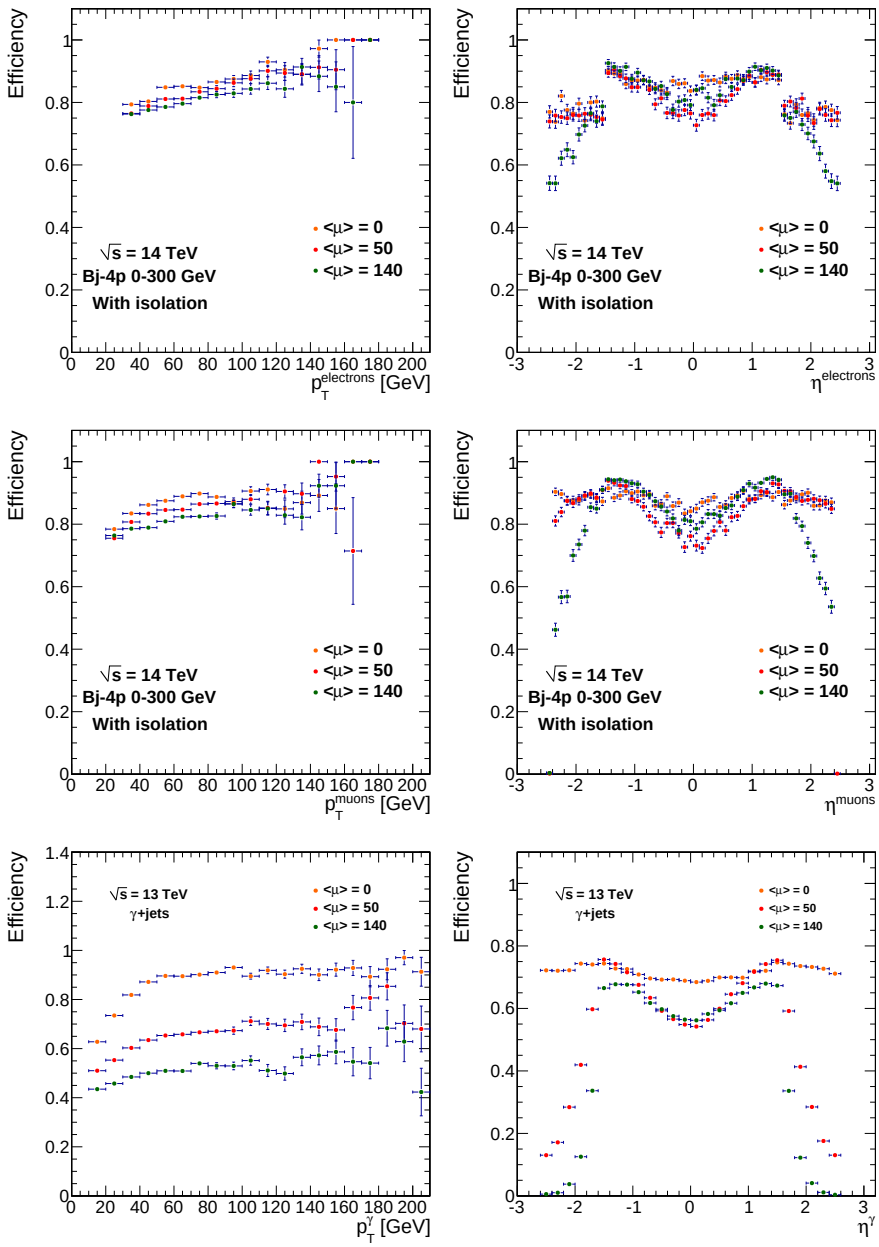

Figure 1-9. *Efficiency for reconstructing isolated electrons (top), muons (middle), and photons (bottom) as functions of p_{T} (left) and η (right).*

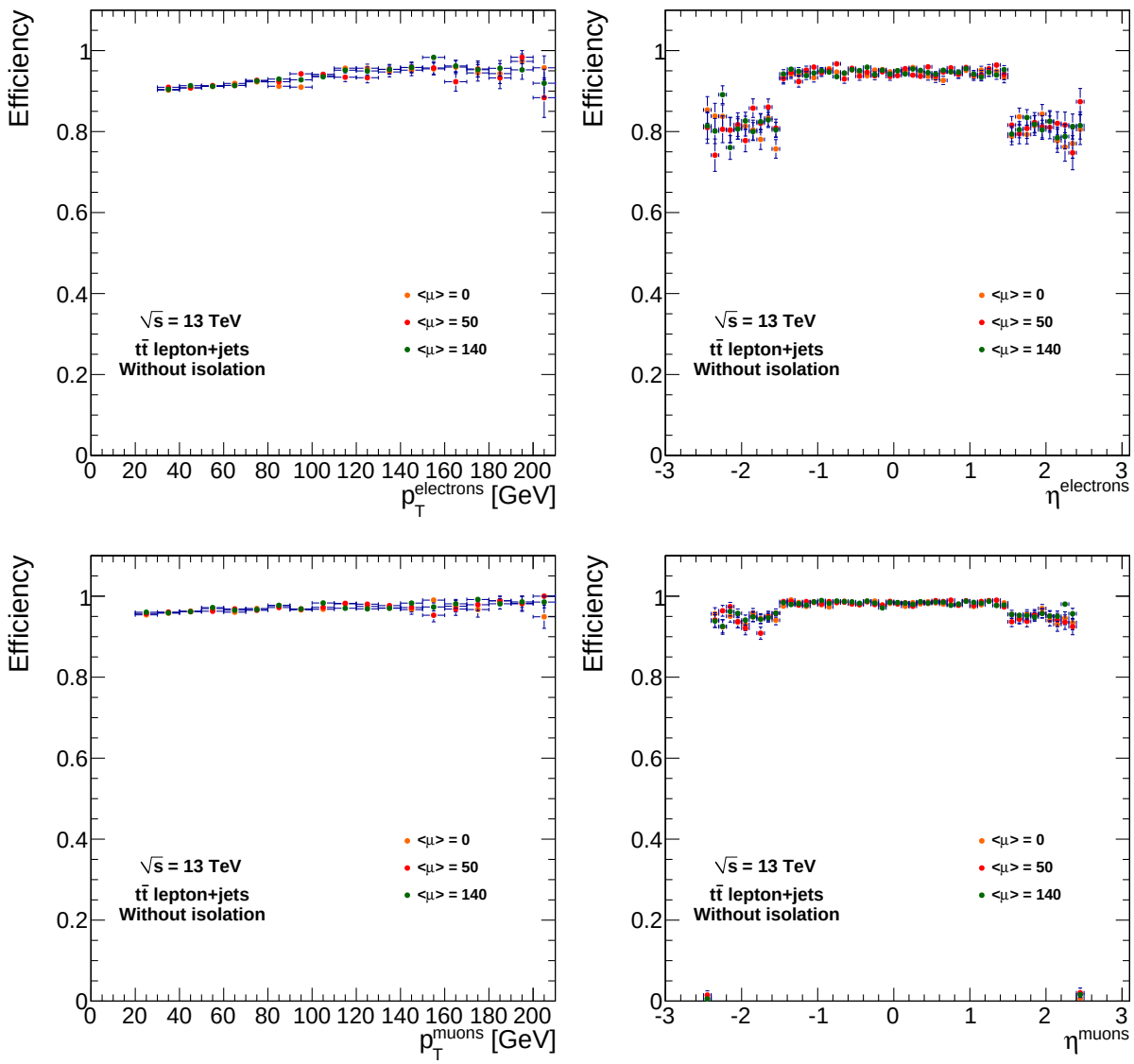

Figure 1-10. *Efficiency for reconstructing electrons (top), muons (middle) as functions of p_T (left) and η (right) with no isolation requirement.*

1.4.3 Jet substructure performance

As described in Sec. 1.3.3.3, top-tagging is based on trimmed jet mass and the number of subjets, and W-tagging is based on trimmed jet mass and mass drop.

Distributions for the number of subjets were already shown above in Fig. 1-4. In Fig. 1-11, we show the mass drop variable for W-tagged jets, and in Fig. 1-12, the trimmed jet mass for top- and W-tagged jets. The effect of pile-up is apparent in the trimmed and untrimmed jet mass in Fig. 1-12: the untrimmed mass decreases with pile-up because of over-correction, while the trimmed mass increases slightly with pile-up.

In Fig. 1-13, we show the top-tagging efficiency as a function of jet p_{T} for several variables. Though the algorithm is stable with different pile-up conditions, it is efficient up to $p_{\mathrm{T}} < 1000$ GeV, the top-tagging efficiency (red curve) degrades for jet p_{T} exceeding 1 TeV. Alternate top-tagging algorithms should be studied in case of analyzes sensitive to very high p_{T} regions.

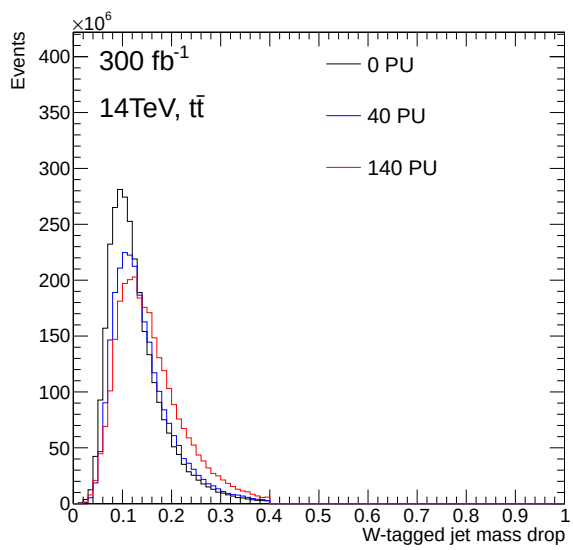

Figure 1-11. *The mass drop variable for $W-$ tagged jets; the top-tagging criteria do not include mass drop.*

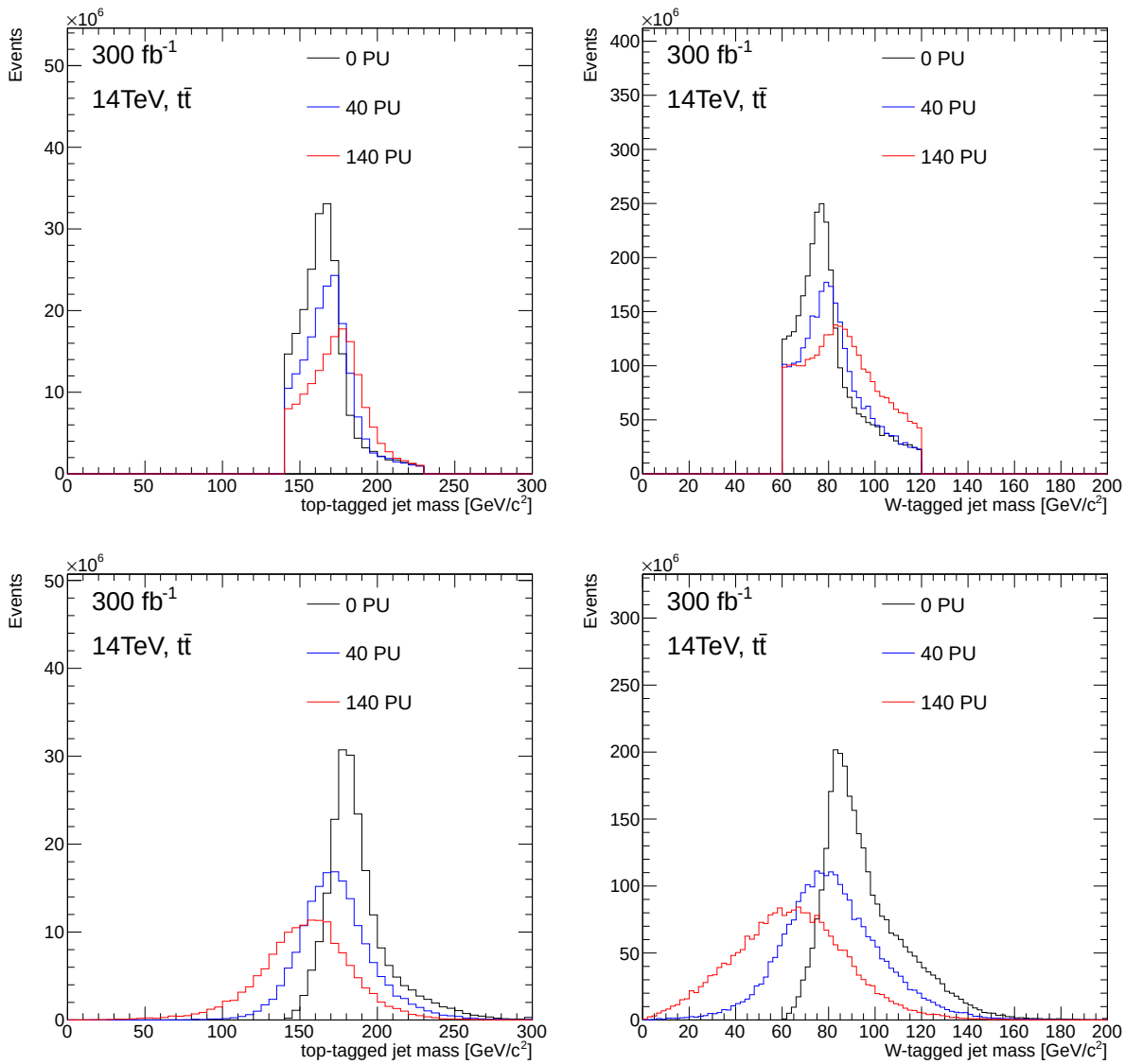

Figure 1-12. *Trimmed jet mass for top-tagged jets (top left) and W-tagged jets (top right) and jet mass for top-tagged jets (bottom left) and W-tagged jets (bottom right).*

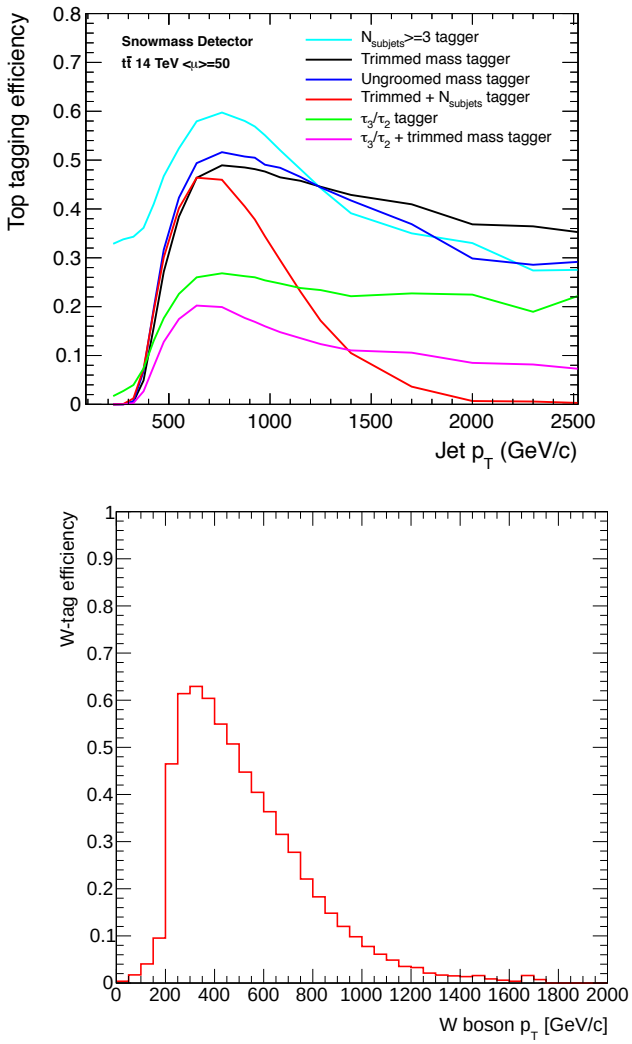

Figure 1-13. *Top-tagging efficiency versus jet p_{T} for taggers based on several combinations of substructure variables (top) and W-tagging efficiency for the default tagger (bottom).*

1.4.4 Performance of b- and τ-tagging

The efficiencies to tag a true b-jet as originating from a b quark or a true τ-jet as originating from a τ lepton, along with the related rates to misidentify a light flavor jet as coming from a b quark or τ lepton, are shown in Figs. 1-14, 1-15, 1-16, 1-17, and 1-18. The measured efficiencies agree well with the inputs used during parametrization.

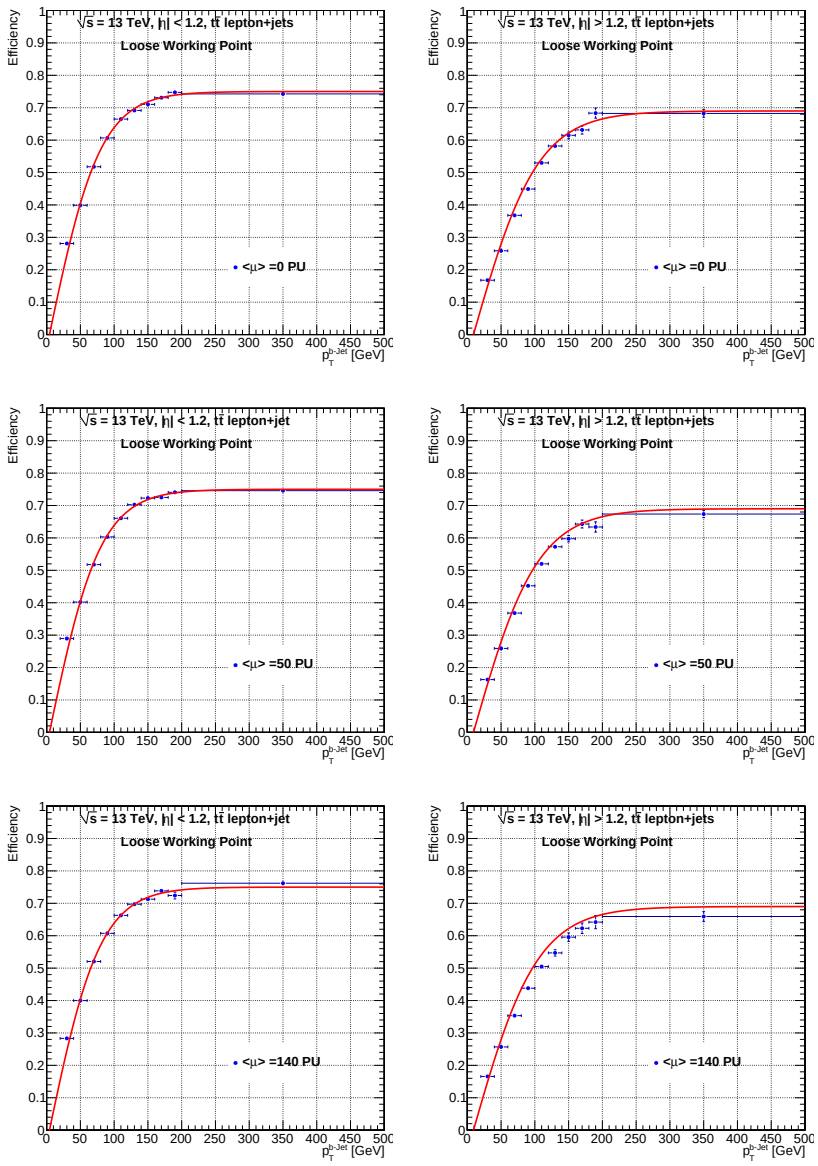

Figure 1-14. Loose working point: *Efficiency for correctly tagging true b quark jets as a function of* p_{T} *for* $|\eta| < 1.2$ *(left) and* $|\eta| > 1.2$ *(right) and for 0 pile-up (top), 50 pile-up (middle), and 140 pile-up (bottom). The curves are the input efficiency parametrization; the points are the measured efficiencies.*

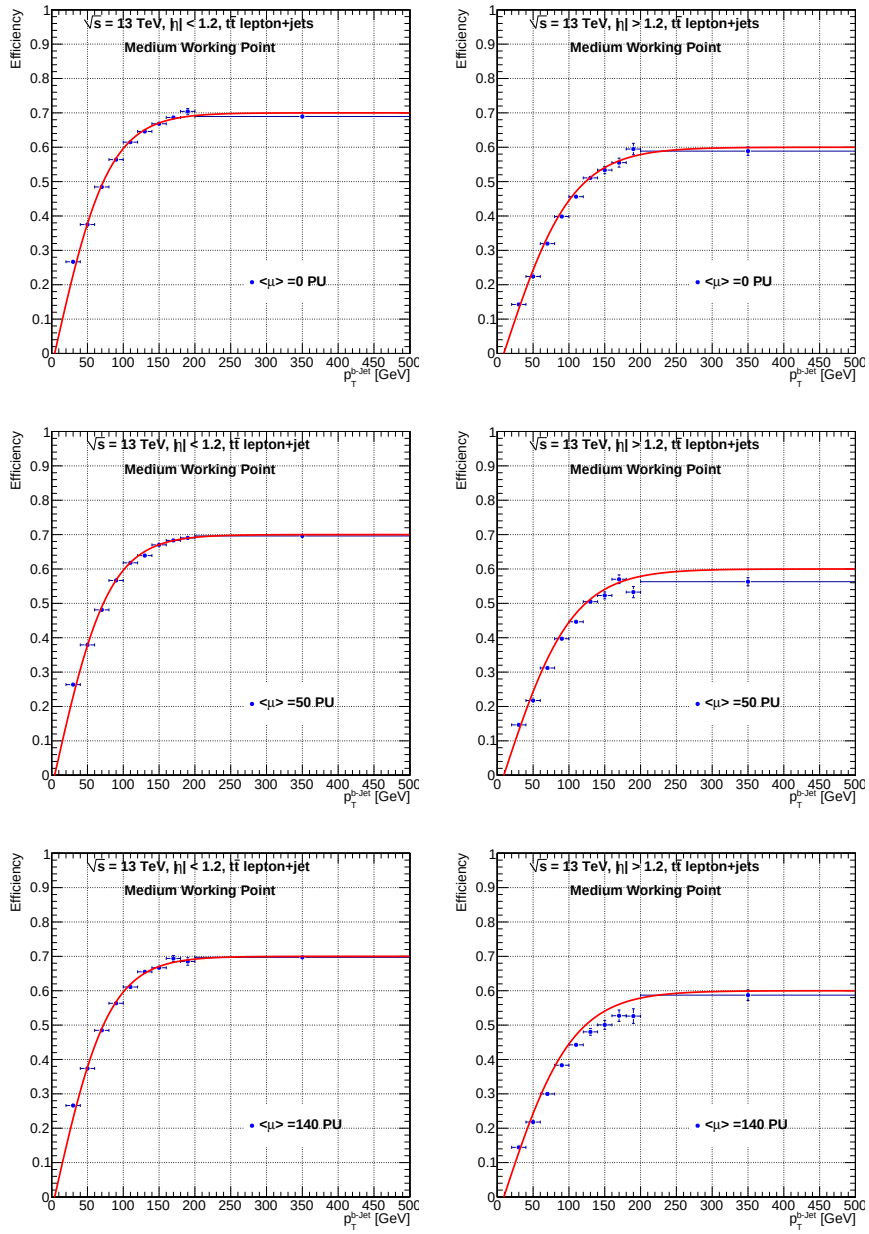

Figure 1-15. Medium working point: *Efficiency for correctly tagging true b quark jets as a function of p_{T} for $|\eta| < 1.2$ (left) and $|\eta| > 1.2$ (right) and for 0 pile-up (top), 50 pile-up (middle), and 140 pile-up (bottom). The curves are the input efficiency parametrization; the points are the measured efficiencies.*

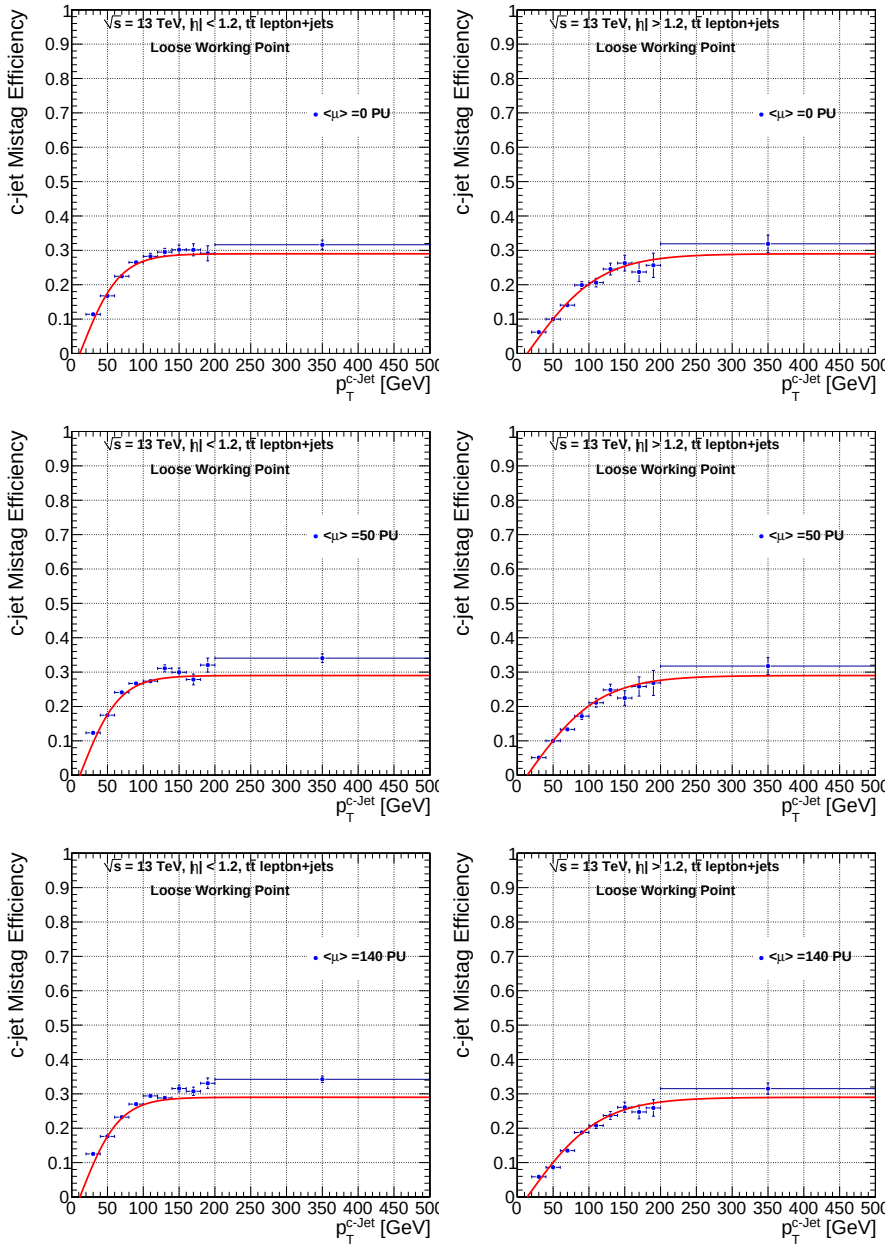

Figure 1-16. Loose working point: *Rate to misidentify a true c quark jet as a b quark jet as a function of* p_{T} *for* $|\eta| < 1.2$ *(left) and* $|\eta| > 1.2$ *(right) and for 0 pile-up (top), 50 pile-up (middle), and 140 pile-up (bottom). The curves are the input efficiency parametrization; the points are the measured efficiencies.*

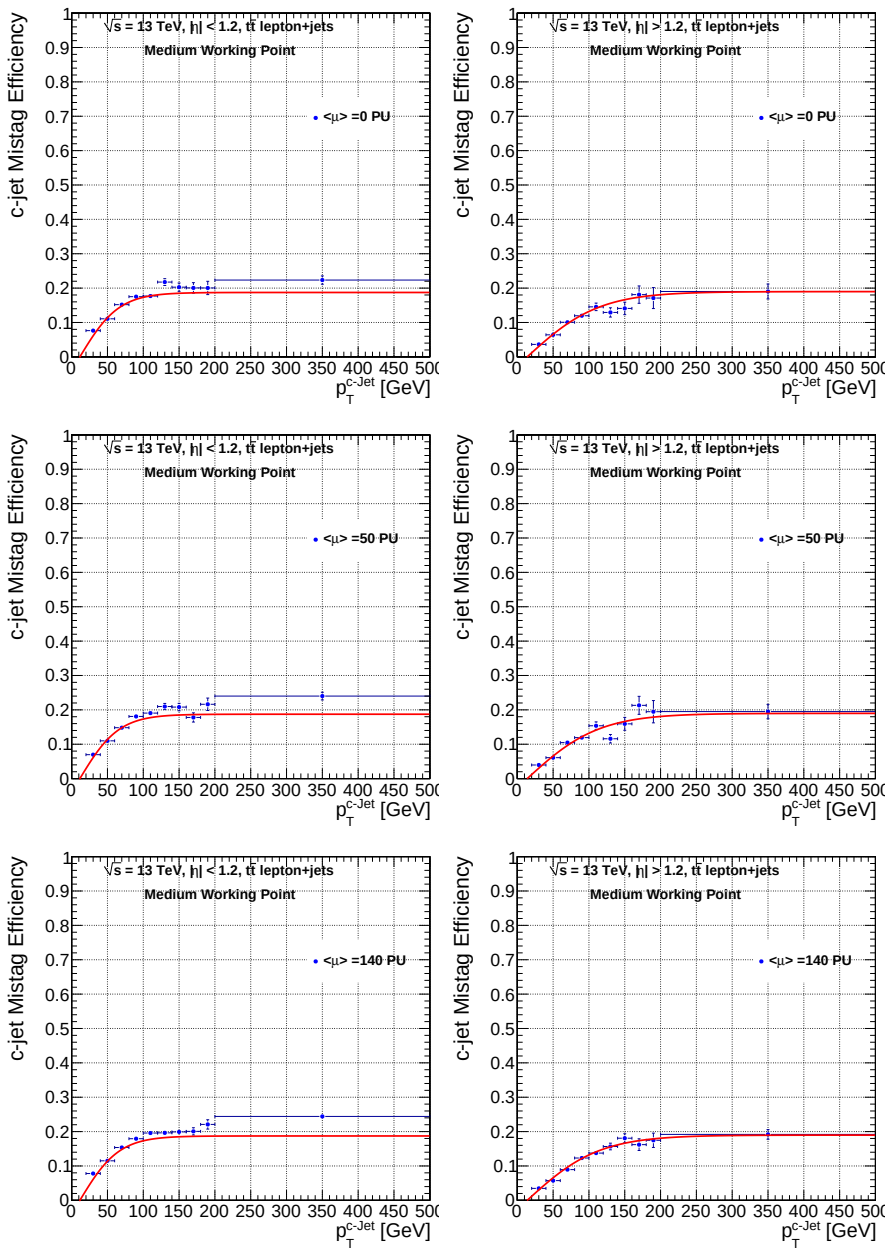

Figure 1-17. Medium working point: *Rate to misidentify a true c quark jet as a b quark jet as a function of* p_{T} *for* $|\eta| < 1.2$ *(left) and* $|\eta| > 1.2$ *(right) and for 0 pile-up (top), 50 pile-up (middle), and 140 pile-up (bottom). The curves are the input efficiency parametrization; the points are the measured efficiencies.*

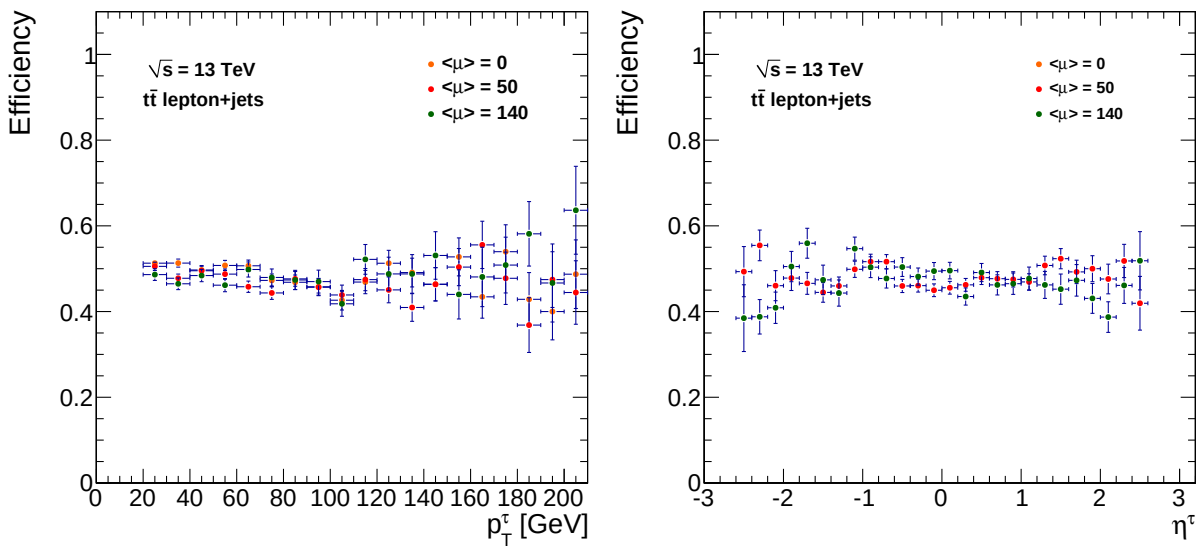

Figure 1-18. *Efficiency for correctly tagging true τ jets as a function p_{T} (left) and η (right).*

1.5 Summary and status

This document describes the simulation framework and reconstructed object performance used in the Snowmass Energy Frontier studies for future Hadron Colliders. For the first time events with large pile-up associated with pp interactions at center-of-mass energies $\sqrt{s}$ = 14, 33, and 100 TeV are studied. Input parametrization for tracks, clusters, as well as reconstructed objects such as leptons, photons, jets etc. are used based on publicly available detector and performance parameters. The study shows a significant impact on lepton, jets and $E_{\mathrm{T}}^{\mathrm{miss}}$ reconstruction due to higher pile-ups expected from the HL-LHC. Pile-up subtraction methods using particle flow for charged hadrons and jet area techniques will be vital for optimal object reconstructions needed for precision physics, as well as searches for new physics at the LHC. Novel techniques are used to simulate large Standard Model backgrounds of 3 ab^{-1} expected due to luminosity evolution of the LHC.

ACKNOWLEDGEMENTS

We thank Beate Heinemann, Joseph Incandela and Michelangelo Manageo for comments and discussions, as well as the Delphes team for support with the software and bug fixes. The studies are done using resources provided by the Open Science Grid, which is supported by the National Science Foundation and the U.S. Department of Energy's Office of Science.

References

[1] ATLAS Collaboration, JINST **03** S08003 (2008).

[2] CMS Collaboration, JINST **03** S08004 (2008).

[3] S. Agostinelli et al., Nucl. Instrum. Meth. A **506** 250 (2003)

[4] J. de Favereau et al., arXiv:1307.6346 [hep-ex] (2013).

[5] CMS Collaboration [http://cds.cern.ch/record/1481838].

[6] ATLAS Collaboration [http://cds.cern.ch/record/1502664].

[7] CMS Collaboration [http://cds.cern.ch/record/1523273].

[8] CMS Collaboration [http://cds.cern.ch/record/1490642].

[9] A. Avetisyan et al., arXiv:1308.1636, Aug. 2013

[10] A. Avetisyan et al., arXiv:1308.0843, Aug. 2013

[11] J. Alwall et al., JHEP **06**, 128 (2011) [arXiv:1106.0522 [hep-ph]].

[12] P. Meade and M. Reece, arXiv:hep-ph/0703031 (2007).

[13] T. Sjöstrand, S. Mrenna, and P. Skands, JHEP **05**, 026 (2006) [arXiv:hep-ph/0603175]

[14] M. Cacciari and G. Salam, Phys. Lett. **B659**, 119 (2008) [arXiv:0707.1378[hep-ph]]

[15] M. Cacciari, G. Salam, and G. Soyez, JHEP **04** 63 (2008) [arXiv:0802.1189[hep-ph]].

[16] M. Wobisch and T. Wengler, arXiv:hep-ph/9907280 (2009).